Acta Crystallographica Section D
Biological Crystallography
ISSN 0907-4449

Structure of the JmjC-domain-containing protein JMJD5

Haipeng Wang,[a,b]‡ Xing Zhou,[a,b]‡ Minhao Wu,[a,b] Chengliang Wang,[a,b] Xiaoqin Zhang,[a,b] Yue Tao,[a,b] Nini Chen[a,b] and Jianye Zang[a,b]*

[a]Hefei National Laboratory for Physical Sciences at Microscale and School of Life Sciences, University of Science and Technology of China, 96 Jinzhai Road, Hefei, Anhui 230026, People's Republic of China, and [b]Key Laboratory of Structural Biology, Chinese Academy of Sciences, Hefei, Anhui 230026, People's Republic of China

‡ These authors contributed equally to this work.

Correspondence e-mail: zangjy@ustc.edu.cn

Received 7 August 2012
Accepted 14 June 2013

PDB Reference: JMJD5, 4gaz

The post-translational modification of histone tails is the principal process controlling epigenetic regulation in eukaryotes. The lysine methylation of histones is dynamically regulated by two distinct classes of enzymes: methyltransferases and demethylases. JMJD5, which plays an important role in cell-cycle progression, circadian rhythms and embryonic cell proliferation, has been shown to be a JmjC-domain-containing histone demethylase with enzymatic activity towards H3K36me2. Here, the crystal structure of human JMJD5 lacking the N-terminal 175 amino-acid residues is reported. The structure showed that the Gln275, Trp310 and Trp414 side chains might block the insertion of methylated lysine into the active centre of JMJD5, suppressing the histone demethylase activity of the truncated JMJD5 construct. A comparison of the structure of JMJD5 with that of FIH, a well characterized protein hydroxylase, revealed that human JMJD5 might function as a protein hydroxylase. The interaction between JMJD5 and the core histone octamer proteins indicated that the histone proteins could be potential substrates for JMJD5.

1. Introduction[1]

Covalent modifications of core histones, including acetylation, methylation, ubiquitination and phosphorylation, have been confirmed to be involved in a variety of cellular processes in eukaryotes, including transcription regulation and chromatin dynamics. Histone lysine methylation is considered to be one of the most complicated modifications because its diverse functions depend on the sites of methylation and the degree of methylation (Martin & Zhang, 2005). Lysine methylation has been identified at six core histone octamer sites: K4, K9, K27, K36 and K79 on histone H3 (H3K4, H3K9, H3K27, H3K36 and H3K79) and K20 on histone H4 (H4K20). Generally, histone methylation at H3K4, H3K36 and H3K79 is thought to be related to transcription activation (Martin & Zhang, 2005; Ng *et al.*, 2003; Xiao *et al.*, 2003; Li *et al.*, 2003), while histones methylated at H3K9 and H3K27 have been shown to be involved in gene silencing (Tachibana *et al.*, 2002; Cao & Zhang, 2004; Martin & Zhang, 2005).

[1] Abbreviations: JmjC, Jumonji C-terminus; JMJD5, JmjC-domain-containing protein 5; H3K36me2, dimethylated lysine 36 of histone H3; FIH, factor inhibiting hypoxia-inducible factor 1; Eaf3, ESA1-associated factor 3; α-KG, α-ketoglutarate; KDM8, histone lysine demethylase 8; NFATc1, nuclear factor of activated T-cells, calcineurin-dependent 1; HIF-1α, hypoxia-inducible factor 1α; NOG, *N*-oxalylglycine; ITC, isothermal titration calorimetry; SAD, single-wavelength anomalous dispersion; IPTG, isopropyl β-D-1-thiogalactopyranoside; JMJD6, JmjC-domain-containing protein 6; U2AF65, the splicing factor U2 small nuclear ribonucleoprotein auxiliary factor 65 kDa subunit.

Methylation of H3K36 has been reported to be associated with gene transcription, alternative splicing, dosage compensation and DNA-damage repair (Wagner & Carpenter, 2012). For example, methylation of H3K36 was shown to be linked to gene activation because actively transcribed genes contained high levels of methylated H3K36 in comparison with inactive genes (Bannister *et al.*, 2005). Another well established function of H3K36 methylation in budding yeast is the suppression of spurious intragenic transcription, which it achieves by recruiting the histone deacetylase complex Rpd3S to the coding region through interaction with the chromodomain-containing subunit Eaf3 (Carrozza *et al.*, 2005). In addition to promoting continuous transcription, it has been demonstrated that H3K36 methylation plays a role in gene repression (Huang *et al.*, 1998; Berdasco *et al.*, 2009). The functional readout of H3K36 methylation is complicated and depends on the surrounding chromatin environment and the proteins recruited in the process.

Histone H3K36 methylation is dynamically regulated by the interplay of histone methyltransferases with demethylases. Several human JmjC-domain-containing histone demethylases have been demonstrated to specifically demethylate histone H3K36 using Fe^{2+} and α-KG as cofactors, including JMJD2A, JMJD2C, JHDM1A, NO66 and JMJD5 (Whetstine *et al.*, 2006; Tsukada *et al.*, 2006; Sinha *et al.*, 2010; Hsia *et al.*, 2010). JMJD5, also known as KDM8, is a newly identified JmjC-domain-containing protein that shows histone demethylase activity towards H3K36me2. It has been shown *in vivo* that JMJD5 acts as a transcriptional activator *via* the demethylation of H3K36me2, resulting in an increased level of histone H3/H4 acetylation. By stimulating the transcription of cyclin A1, JMJD5 facilitates progression in the cell cycle that is critical for cancer cell proliferation (Hsia *et al.*, 2010). In addition, JMJD5 gene-knockout mice showed severe embryonic growth retardation (Ishimura *et al.*, 2012). Furthermore, JMJD5 was found to play an important role in the circadian systems of *Arabidopsis* and humans (Jones *et al.*, 2010; Jones & Harmer, 2011). It is worth mentioning that JMJD5 has been identified as a hydroxylase in mice. JMJD5 functions as a novel osteoclastogenic repressor by inducing the degradation of NFATc1, a necessary and sufficient transcription factor for osteoclasogenesis, *via* its hydroxylase activity (Youn *et al.*, 2012). Therefore, the question of whether human JMJD5 is a histone demethylase remains controversial.

In this context, we purified and crystallized recombinant human JMJD5 (containing amino-acid residues 176 to the C-terminus, referred to as JMJD5$^{176\text{-}C}$). The JMJD5$^{176\text{-}C}$ crystals diffracted to a resolution of 2.8 Å. Our structure revealed that the JmjC domain of JMJD5 adopts a conserved jelly-roll-like fold. However, three residues within the JmjC domain of JMJD5 were found to occupy the entrance to the active pocket, thereby preventing the binding of dimethylated lysine residues in comparison with the structures of PHF8 and ceKDM7A in complex with dimethylated histone substrates. Comparing the structure of JMJD5 with that of FIH indicated that JMJD5 might act as a protein hydroxylase.

2. Methods

2.1. Protein expression, purification and crystallization

The DNA fragment coding JMJD5$^{176\text{-}C}$ was amplified using PCR and ligated into pET-24a (Novagen) vector with a 6×His tag fused to its C-terminus, pET-28a (Novagen) vector with a SUMO tag fused to its N-terminus or pGEX-6p-1 (GE Healthcare) vector. The proteins were overexpressed in *Escherichia coli* Rosetta2 (DE3) cells (Novagen). The cells were grown at 310 K until the $OD_{600\ nm}$ reached 0.6, and then protein overexpression was induced *via* incubation with 0.4 m*M* IPTG for 20 h at 289 K.

The cells containing JMJD5$^{176\text{-}C}$ with a 6×His tag fused to the C-terminus were harvested and lysed in lysis buffer (20 m*M* Tris–HCl pH 8.0, 500 m*M* NaCl, 5% glycerol, 3 m*M* imidazole) using sonication. After centrifugation, the supernatant was passed through an Ni–NTA Superflow column (Qiagen). The column was then washed using washing buffer (20 m*M* Tris–HCl pH 8.0, 500 m*M* NaCl, 5% glycerol, 30 m*M* imidazole) and the target protein was eluted with elution buffer (20 m*M* Tris–HCl pH 8.0, 500 m*M* NaCl, 5% glycerol, 300 m*M* imidazole). The protein was further purified using a HiLoad 16/60 Superdex 200 size-exclusion column (GE Healthcare) in buffer *A* (50 m*M* Tris–HCl pH 8.0, 100 m*M* NaCl). The eluted fraction corresponding to the JMJD5$^{176\text{-}C}$ monomer was collected and concentrated for further use.

Selenomethionine-labelled JMJD5$^{176\text{-}C}$ (Se-JMJD5$^{176\text{-}C}$) was expressed in *E. coli* Rosetta2 (DE3) cells in M9 medium supplemented with selenomethionine (Sigma–Aldrich) at a final concentration of 60 mg l^{-1} using the methionine-biosynthesis inhibition method. Se-JMJD5$^{176\text{-}C}$ was purified using the protocol used for native JMJD5$^{176\text{-}C}$ purification.

The JMJD5$^{176\text{-}C}$ protein with a SUMO tag fused at the N-terminus was purified using the protocol used for native JMJD5$^{176\text{-}C}$ purification. The His-SUMO tag was removed using SUMO protease at 277 K overnight. The cleaved protein mixture was loaded onto an Ni–NTA Superflow column (Qiagen). The flowthrough fraction was further purified using a HiLoad 16/60 Superdex 200 size-exclusion column (GE healthcare) equlibrated with buffer *A*.

The cells containing GST-JMJD5$^{176\text{-}C}$ were lysed *via* sonication in buffer *B* (50 m*M* Tris–HCl pH 8.0, 500 m*M* NaCl, 5% glycerol). After centrifugation, the supernatant fraction was incubated with GST resin (GE Healthcare) at 277 K for 1 h. The resin was washed with buffer *B* and GST-JMJD5$^{176\text{-}C}$ was eluted using 10 m*M* glutathione (Songon) in buffer *B*. The eluted GST-JMJD5$^{176\text{-}C}$ was further purified using a HiLoad 16/60 Superdex 200 size-exclusion column (GE Healthcare) in buffer *A* (50 m*M* Tris–HCl pH 8.0, 100 m*M* NaCl). The eluted protein was collected and concentrated for further use.

2.2. Crystallization

Crystals of native JMJD5$^{176\text{-}C}$ and Se-JMJD5$^{176\text{-}C}$ were obtained using the sitting-drop vapour-diffusion method. Before crystallization, NOG was added to the protein solution to give a final protein:NOG molar ratio of 1:4. 1 µl native JMJD5$^{176\text{-}C}$ (16 mg ml^{-1}) or Se-JMJD5$^{176\text{-}C}$ (20 mg ml^{-1})

Table 1
Data-collection and refinement statistics.

Values in parentheses are for the highest resolution shell.

	Se-JMJD5$^{176\text{-}C}$	Native JMJD5$^{176\text{-}C}$
Data collection		
Space group	$P3_121$	$P3_221$
Unit-cell parameters		
$a = b$ (Å)	69.43	69.431
c (Å)	267.95	270.052
$\alpha = \beta$ (°)	90	90
γ (°)	120	120
Wavelength (Å)	0.9792	0.9792
Resolution (Å)	3.50 (3.69–3.50)	2.80 (2.90–2.80)
No. of unique reflections	9227 (1052)	19419 (1899)
$R_{\rm merge}$† (%)	9.6 (24.5)	7.0 (32.5)
$\langle I/\sigma(I)\rangle$	19.5 (9.0)	24.1 (5.3)
Completeness (%)	90.8 (73.6)	94.6 (99.0)
Multiplicity	11.2 (10.7)	4.5 (4.8)
Wilson B factor (Å^2)	77.8	90.0
Refinement		
$R_{\rm work}$‡ (%)		22.07
$R_{\rm free}$§ (%)		27.40
No. of atoms		
Protein		3856
Water		17
Ni^{2+}		2
NOG		20
Average B factors (Å^2)		
Protein		82.0
Water		79.09
Ni^{2+}		84.35
NOG		77.01
R.m.s. deviations		
Bond lengths (Å)		0.009
Bond angles (°)		1.187
Ramachandran plot, residues in		
Most favoured regions (%)		93.3
Additional allowed regions (%)		6.7
Disallowed regions (%)		0

† $R_{\rm merge} = \sum_{hkl}\sum_i |I_i(hkl) - \langle I(hkl)\rangle| / \sum_{hkl}\sum_i I_i(hkl)$, where $I_i(hkl)$ is the intensity of the ith measurement of reflection hkl and $\langle I(hkl)\rangle$ is the mean intensity for reflection hkl. ‡ $R_{\rm work} = \sum_{hkl} \big||F_{\rm obs}| - |F_{\rm calc}|\big| / \sum_{hkl} |F_{\rm obs}|$, where $|F_{\rm obs}|$ and $|F_{\rm calc}|$ are the observed and calculated structure-factor amplitudes, respectively. § $R_{\rm free}$ was calculated with 5.0% of the reflections as a test set.

solution was mixed with 1 µl of a well solution consisting of 100 m*M* HEPES pH 7.5, 9%(*v*/*v*) PEG 3350, 1 m*M* $NiCl_2$. The mixture was equilibrated against 100 µl well solution at 289 K. Single crystals were obtained after 4 d.

2.3. Data collection, structure determination and refinement

The crystals were soaked in a cryoprotectant solution consisting of well solution and 25%(*v*/*v*) glycerol and flash-cooled in liquid nitrogen. X-ray diffraction data were collected at 100 K on the BL17U1 beamline at SSRF, Shanghai. The diffraction data for the Se-JMJD5$^{176\text{-}C}$ crystals were processed using *iMosflm* (Battye *et al.*, 2011), *POINTLESS* and *SCALA* (Evans, 2006) from the *CCP*4 suite (Winn *et al.*, 2011). The diffraction data for native JMJD5$^{176\text{-}C}$ were indexed, integrated and scaled using *HKL*-2000 (Otwinowski & Minor, 1997).

The structure of JMJD5$^{176\text{-}C}$ was solved using the SAD method. The initial phases were calculated using *AutoSol* and the structural model was built automatically using *AutoBuild* in *PHENIX* (Adams *et al.*, 2002). Molecular replacement was performed using the initial JMJD5$^{176\text{-}C}$ structure as the search model against the diffraction data for native JMJD5$^{176\text{-}C}$ with *Phaser* (McCoy *et al.*, 2007). The structural model was manually refined to 2.8 Å resolution using *Coot* and *REFMAC*5 (Murshudov *et al.*, 2011; Emsley & Cowtan, 2004) with an R factor of 22.07% ($R_{\rm free}$ = 27.40%). The final model was validated using *PROCHECK* (Laskowski *et al.*, 1993). The statistics of data processing and structure refinement are listed in Table 1.

2.4. ITC assay

Isothermal titration calorimetry measurements were performed as reported previously (Ruan *et al.*, 2012). Experiments were carried out by injecting 40 µl peptide solution (3.2 m*M*) into a sample cell containing 80 µ*M* JMJD5$^{176\text{-}C}$ protein (without any tags) in buffer *A*. The ITC measurements were analysed using *Origin* (MicroCal Inc.). The synthesized peptides used were H3K36 (APATGGVKKPHRYRP), H3K36me (ATGGVK$_{\rm me}$KPHR), H3K36me2 (ATGGVK$_{\rm me2}$KPHR) and H3K36me3 (ATGGVK$_{\rm me3}$KPHR) (SciLight Biotechnology).

2.5. Demethylation activity assay

20 µg JMJD5$^{176\text{-}C}$ was incubated with 20 µg calf thymus bulk histones (Worthington), 50 µ*M* ammonium sulfate, 1 m*M* α-KG, 2 m*M* ascorbic acid for 4 h at 310 K. The reaction was terminated *via* the addition of 2× SDS loading buffer and the protein mixture was separated by SDS–PAGE. The protein samples were electroblotted onto a PVDF membrane and visualized immunochemically using standard methods. Immunodetection was performed using an enhanced chemiluminescence kit (Thermo). The antibodies used as probes were the primary antibodies anti-histone H3 (Abcam) and anti-H3K36me2 (Active Motif) and the secondary antibody goat anti-mouse IgG, HRP conjugate (Thermo).

2.6. Pulldown assays

Purified GST-JMJD5$^{176\text{-}C}$ was incubated with 20 µl glutathione Sepharose beads pre-equilibrated with buffer *C* (PBS, 0.01% Triton X-100). The GST-JMJD5$^{176\text{-}C}$ immobilized with glutathione Sepharose beads was incubated with calf thymus bulk histones (Worthington) in buffer *C*. After incubation at 277 K for 1 h, the beads were washed with buffer *C* five times. The beads were boiled with SDS sample buffer and the proteins retained on the glutathione Sepharose beads were analysed using SDS–PAGE.

3. Results and discussion

3.1. Overall structure of JMJD5$^{176\text{-}C}$

There are two isoforms of JMJD5, isoforms 1 and 2, in humans, which contain 454 and 416 amino-acid residues, respectively. Here, we report the crystal structure of the truncated construct JMJD5$^{176\text{-}C}$ of isoform 2 fused with a 6×His tag at its C-terminus. After screening several constructs

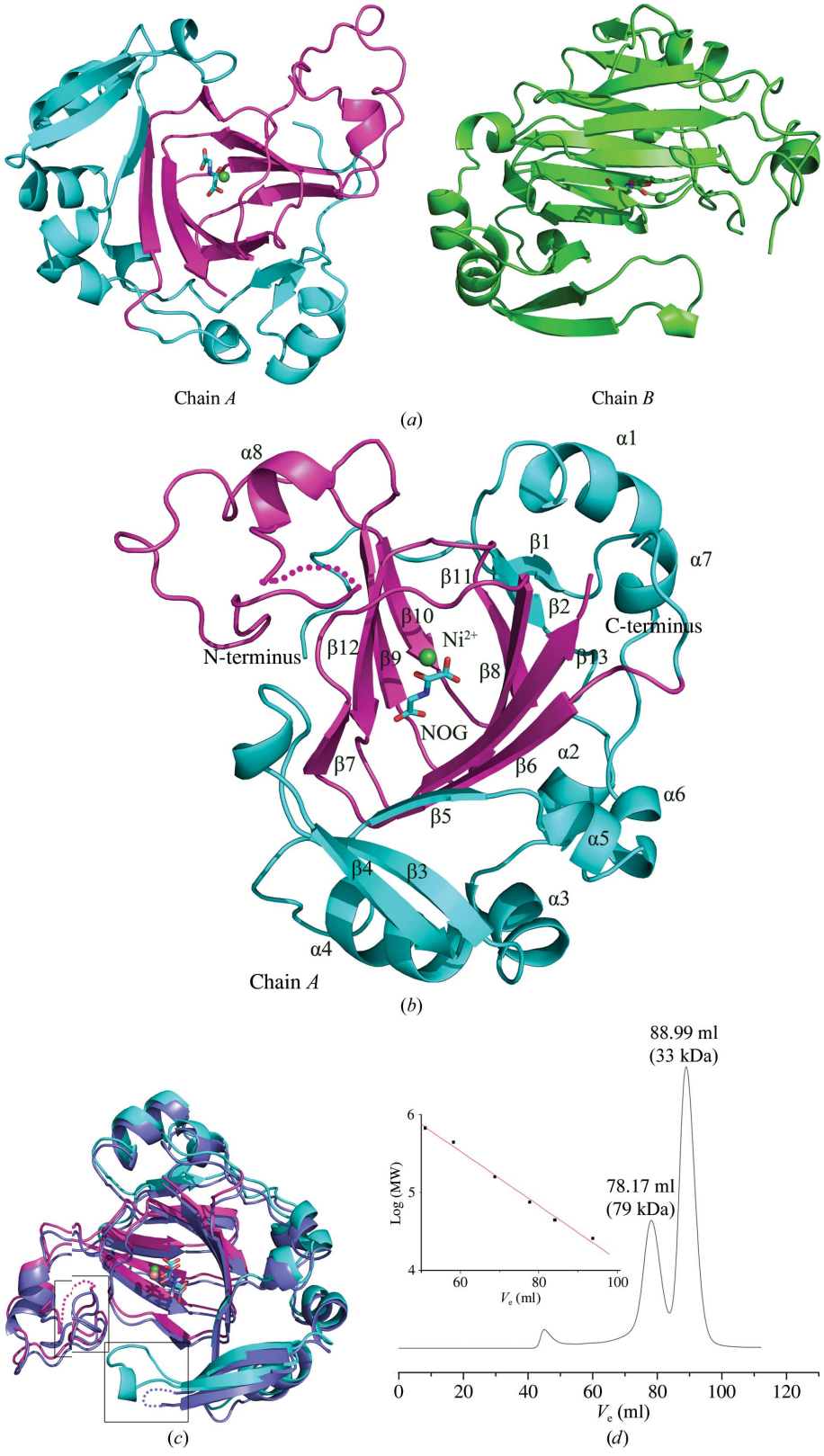

Figure 1
Overall structure of JMJD5$^{176\text{-}C}$. (*a*) Ribbon representation of two JMJD5$^{176\text{-}C}$ molecules in one asymmetric unit. The JmjC domain of chain *A* is coloured magenta and the other part is coloured cyan. Ni^{2+} is shown as a sphere and is coloured green. NOG is shown as a stick model. Chain *B* is coloured green. (*b*) Ribbon representation of the overall structure of the JMJD5$^{176\text{-}C}$ monomer. The molecule is coloured the same as chain *A* in (*a*). (*c*) Superimposition of the structure of JMJD5$^{176\text{-}C}$ with that of JMJD5$^{183\text{-}C}$ (PDB entry 4gjy; Del Rizzo *et al.*, 2012). JMJD5$^{183\text{-}C}$ is coloured blue and JMJD5$^{176\text{-}C}$ is coloured the same as chain *A* in (*a*). The two different regions are indicated by black boxes. (*d*) Size-exclusion chromatography of JMJD5$^{176\text{-}C}$. Blue dextron 2000 (V_e = 48.45 ml), ferritin (440 kDa; V_e = 59.38 ml), aldolase (158 kDa; V_e = 69.09 ml), conalbumin (75 kDa; V_e = 78.03 ml), ovalbumin (44 kDa; V_e = 83.83 ml) and chymotrypsinogen A (25.7 kDa; V_e = 93.54 ml) were used as molecular-weight markers.

containing different regions of JMJD5, we finally found that the fragment lacking the first 175 residues could be prepared on a large scale and formed single crystals that were suitable for X-ray diffraction studies. JMJD5$^{176\text{-}C}$ was crystallized in complex with Ni^{2+} and NOG, an inactive analogue of α-KG, in space group $P3_221$. The phase problem was solved using the SAD method in combination with molecular replacement. The statistics of X-ray diffraction data collection and structure refinement are shown in Table 1.

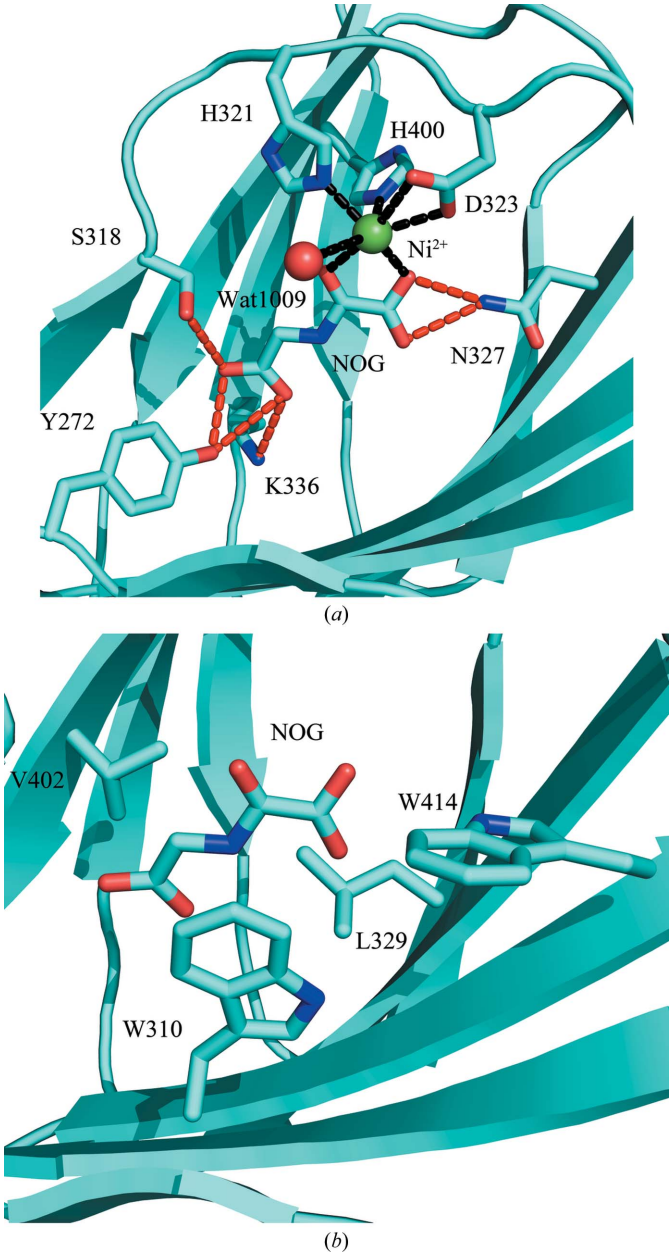

Figure 2
The active site of JMJD5. (*a*) Coordination of Ni^{2+} and polar interactions between NOG and JMJD5. NOG and the residues involved in the binding of Ni^{2+} and NOG are shown as stick models. Ni^{2+} and a water molecule are shown as spheres and are coloured green and red, respectively. (*b*) The hydrophobic interactions between NOG and JMJD5. NOG and the residues that make hydrophobic interactions with NOG are shown as stick models.

Two JMJD5$^{176\text{-}C}$ molecules were present in one crystallographic asymmetric unit with similar conformations, as confirmed by the fact that the root-mean-square deviation (r.m.s.d.) was 0.2 Å on comparing all C^{α} atoms (Fig. 1*a*). JMJD5$^{176\text{-}C}$ was eluted from the size-exclusion column as two peaks with apparent molecular weights of 33 and 79 kDa, respectively (Fig. 1*d*). The theoretical molecular weight of JMJD5$^{176\text{-}C}$ is 29 kDa. JMJD5$^{176\text{-}C}$ exists in monomeric and dimeric oligomerization states in solution. However, the majority of JMJD5$^{176\text{-}C}$ in solution was in the monomeric state (Fig. 1*d*). The buried surface area of the dimer interface was approximately 130 Å^2, indicating that the monomeric state was more stable in solution than the dimeric state. Another possibility is that we only obtained crystals of the JMJD5$^{176\text{-}C}$ monomer and the structure of JMJD5$^{176\text{-}C}$ that we have determined only represents the monomeric state of JMJD5 in solution.

The central core of the catalytic domain (residues 271–416) of JMJD5$^{176\text{-}C}$ adopts a jelly-roll-like scaffold formed by eight β-strands (β6–β13). The active site is located in the centre of the jelly-roll-like fold, which is similar to other JmjC-domain-containing oxygenases (Hou & Yu, 2010). Furthermore, the jelly-roll-like fold is surrounded by additional β-strands (β1–β5) and α-helices (α1–α7). The additional five β-strands (β1–β5) form a nine-stranded antiparallel β-sheet, with four β-strands of the jelly-roll-like fold on one side. Seven additional helices (α1–α7) at the N-terminus are located on the side of the nine-stranded β-sheet and helix α8 lies on the other side of the jelly-roll-like structure (Fig. 1*b*).

Recently, a crystal structure was reported of JMJD5 (containing residues 183 to the C-terminus, referred to as JMJD5$^{183\text{-}C}$; Del Rizzo *et al.*, 2012). The overall structure of JMJD5$^{176\text{-}C}$ is similar to JMJD5$^{183\text{-}C}$, with an r.m.s.d. value of 0.6 Å for 228 aligned C^{α} atoms. The fragment between residues 353 and 358 is disordered in the structure of JMJD5$^{176\text{-}C}$ and is ordered in JMJD5$^{183\text{-}C}$ (Fig. 1*c*). In addition, the loop connecting β3 and β4 is ordered in the structure of JMJD5$^{176\text{-}C}$ and is disordered in JMJD5$^{183\text{-}C}$ (Fig. 1*c*). These observations reveal the high flexibility of these regions.

3.2. The active site of JMJD5$^{176\text{-}C}$

The active site of the JmjC-domain-containing histone demethylase is located in the centre of the jelly-roll-like fold and the Fe^{2+}-binding site is composed of a highly conserved H-*X*-D/E-X_n-H motif (Klose *et al.*, 2006). In the structure of JMJD5$^{176\text{-}C}$, Ni^{2+} and NOG were observed in the active centre. Ni^{2+} was modelled in the Fe^{2+}-binding site because Ni^{2+} was added during crystallization. The conserved H-*X*-D/E-X_n-H motif was identified in the structure of JMJD5$^{176\text{-}C}$ and consisted of His321, Asp323 and His400, providing the chemical groups to chelate Ni^{2+}. In addition, one water molecule and two NOG carbonyl groups were involved in the coordination of Ni^{2+} (Fig. 2*a*). NOG was tethered by two conserved residues: Tyr272 and Lys336. The ε-amino group of Lys336 and the hydroxyl group of Tyr272 formed hydrogen bonds to the C5 carboxyl and hydroxyl groups of NOG.

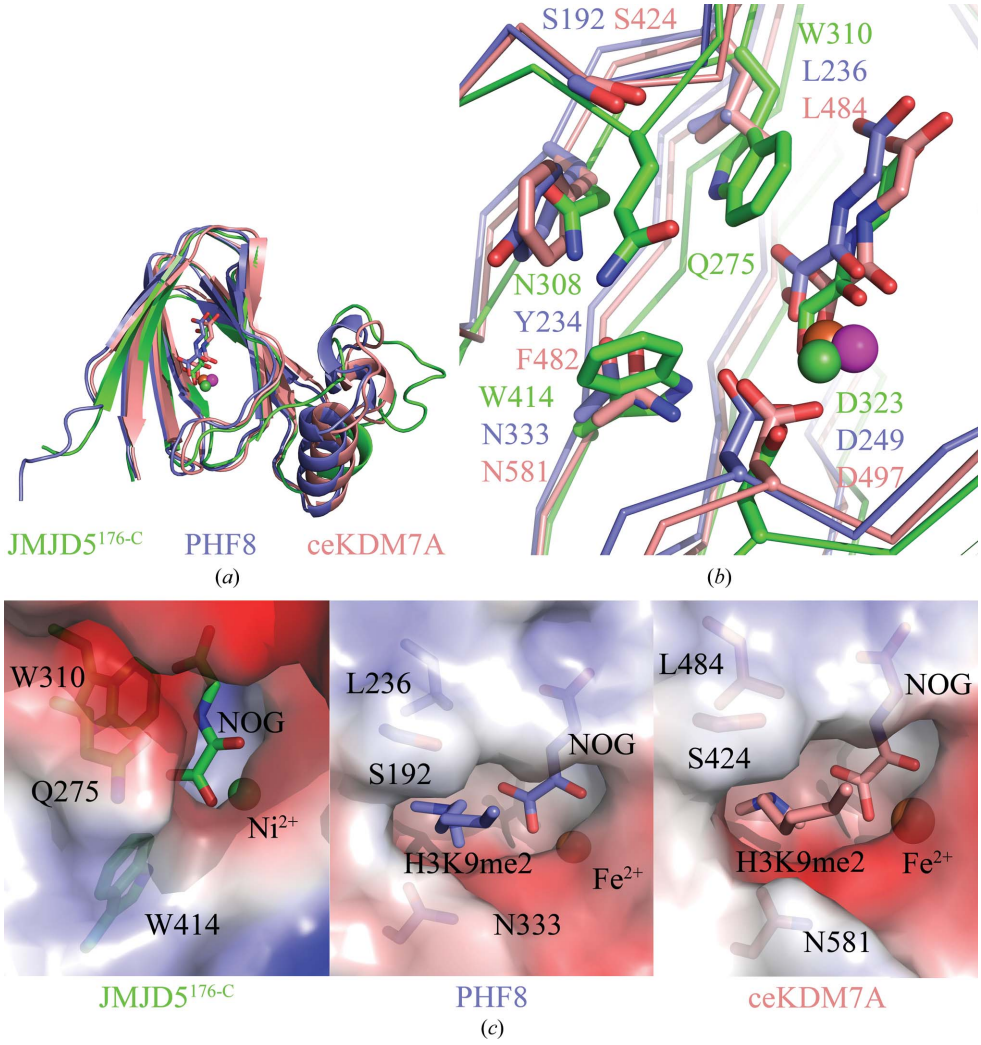

Figure 3
Structural comparison of the JmjC domain of JMJD5 with those of PHF8 and ceKDM7A. (*a*) Superimposition of the JmjC domain of JMJD5 with those of PHF8 (PDB entry 3kv4; Horton *et al.*, 2010) and ceKDM7A (PDB entry 3n9n; Yang *et al.*, 2010). (*b*) Comparison of the substrate-binding pockets of JMJD5, PHF8 and ceKDM7A. (*c*) Surface representation of the substrate-binding pockets of JMJD5$^{176\text{-}C}$ (left panel), PHF8 (middle panel) and ceKDM7A (right panel). NOG, the methylated lysine residues and the residues located at the entrance of the substrate-binding pockets are shown as stick models. The metal ions are shown as spheres. The white, blue and red regions indicate neutral areas, positively charged areas and negatively charged areas, respectively. JMJD5, PHF8 and ceKDM7A are coloured green, light blue and salmon, respectively.

Residues Ser318 and Asn327 in the JmjC domain of JMJD5$^{176\text{-}C}$ also formed hydrogen bonds to NOG (Fig. 2*a*). Moreover, residues Trp310, Leu329, Val402 and Trp414 interacted with NOG *via* hydrophobic contacts (Fig. 2*b*). NOG was fixed in the binding site of JMJD5 through hydrogen bonds and hydrophobic interactions.

3.3. Structural comparisons with other JmjC-domain-containing proteins

As a recently identified JmjC-domain-containing protein, JMJD5 is believed to be an H3K36me2-specific demethylase (Hsia *et al.*, 2010). To date, dozens of JmjC-domain-containing histone demethylases have been characterized, including PHF8 and ceKDM7A, which recognize dimethylated histone substrates (Yang *et al.*, 2010; Horton *et al.*, 2010). We therefore compared the JmjC-domain structure of JMJD5 with these two enzymes. The superimposition of the three structures indicated that all of the JmjC domains in the three proteins adopted similar scaffolds, except for the insertions between the fourth and fifth β-strands of the jelly-roll-like fold. The r.m.s.d. values are 2.5 and 2.4 Å for aligned C$^{\alpha}$ atoms of PHF8 (109 C$^{\alpha}$ atoms) and ceKDM7A (103 C$^{\alpha}$ atoms) relative to JMJD5$^{176\text{-}C}$, respectively (Fig. 3*a*).

The methylated lysine-binding modes are similar in the complex structures formed by PHF8 and ceKDM7A with their substrates (Yang *et al.*, 2010; Horton *et al.*, 2010). In all PHF8 and ceKDM7A complex structures the distances between the ε-amino group of the methylated lysine and the C1 atom of NOG range from approximately 3 to 4 Å and the two methyl groups are distant from the active centre. There is no room to accommodate another methyl group because of the steric hindrance effect. This helps PHF8 and ceKDM7A to discriminate between dimethylated and trimethylated histone substrates (Horton *et al.*, 2010; Yang *et al.*, 2010). The active pockets Asn333, Asp249 and Tyr234 of PHF8 and Asn581, Ala497 and Phe482 of ceKDM7A are involved in interactions with methylated lysine residues (Horton *et al.*, 2010; Yang *et al.*, 2010). In JMJD5, the corresponding residues are Trp414, Asp323 and Asn308, resulting in a different pocket for substrate binding (Fig. 3*b* and Supplementary Fig. S1[2]). Further analysis of the structure of JMJD5$^{176\text{-}C}$ demonstrated that the side chains of Gln275, Trp310 and Trp414 occupy positions around the entrance of the substrate-binding pocket in the JmjC domain of JMJD5. The corresponding residues in the structures of PHF8 and ceKDM7A in complex with methylated peptides are Ser192, Leu236 and Asn333, and Ser424, Leu484 and Asn581, respectively (Fig. 3*b* and Supplementary Fig. S1). The side

[2] Supplementary material has been deposited in the IUCr electronic archive (Reference: XB5066). Services for accessing this material are described at the back of the journal.

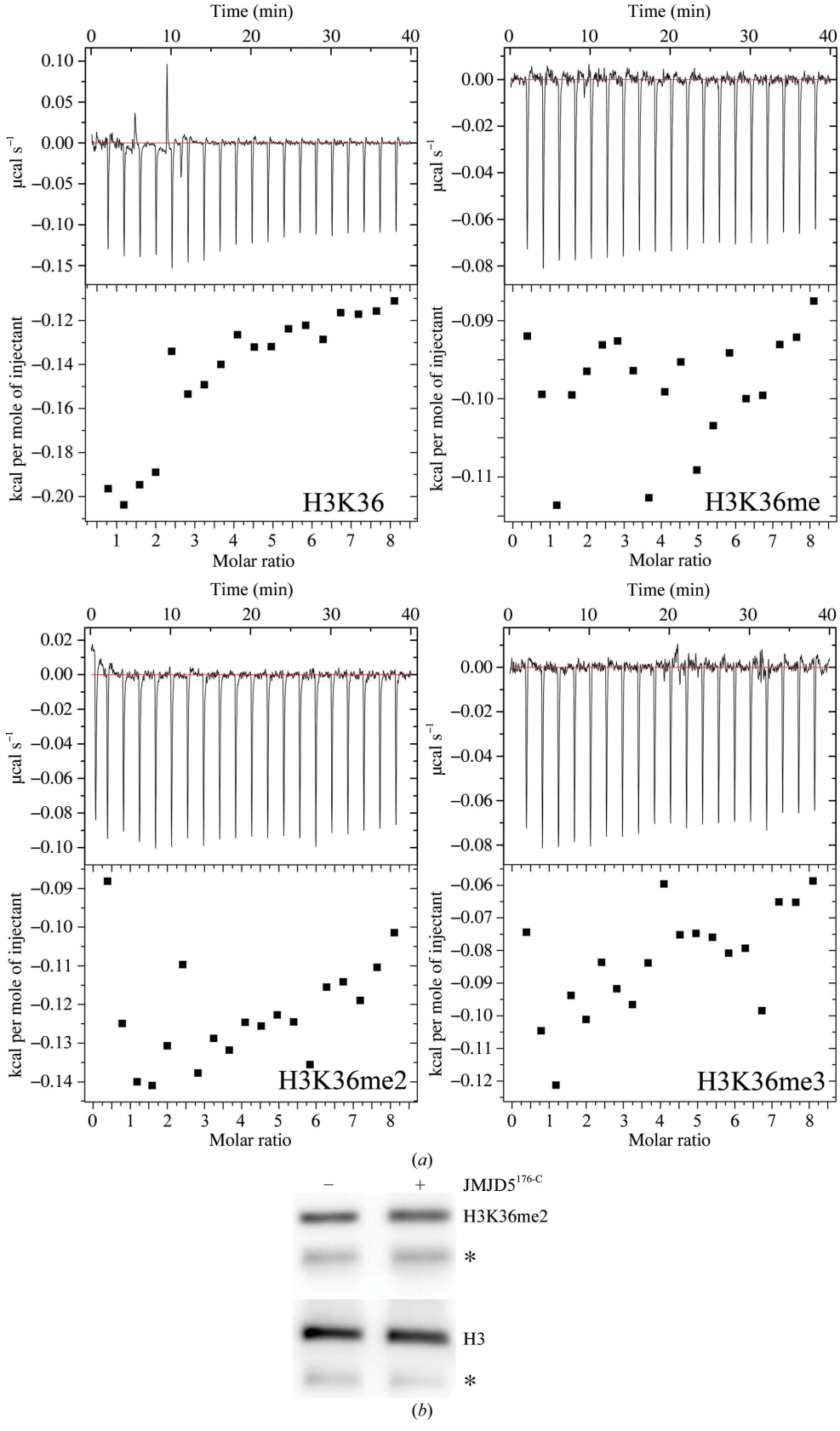

Figure 4
JMJD5^{176-C} has no histone H3K36me2 demethylase activity. (*a*) ITC data for JMJD5^{176-C} binding to H3K36 peptides. The lower panel shows the fit of a single-site binding model to the binding isotherms. (*b*) The histone demethylase activity was assayed using recombinant JMJD5^{176-C} and calf thymus bulk histones; this was followed by immunoblotting with anti-H3K36me2 antibodies. Asterisks indicate nonspecific bands.

chains of these residues of PHF8 and ceKDM7A are smaller than those of JMJD5. As a result, the entrance to the substrate-binding pocket in JMJD5 is much narrower than in PHF8 or ceKDM7A (Fig. 3*c*). The narrow entrance might act as a barrier, blocking the insertion of the methylated lysine residue into the active centre in JMJD5. Consistent with this hypothesis, we failed to detect any interactions between JMJD5^{176-C} and four different H3K36 peptides (unmethylated, monomethylated, dimethylated and trimethylated; Fig. 4*a*). In addition, the results of an enzymatic assay revealed that JMJD5^{176-C} did not display any demethylation activity towards H3K36me2 *in vitro* (Fig. 4*b*). Taken together, the structural and biochemical analyses indicated that JMJD5^{176-C} is enzymatically inactive as a histone H3K36me2 demethylase. It has previously been reported that JMJD5 is capable of demethylating H3K36me2 *in vivo*, and a construct encoding residues 101 to the C-terminus of JMJD5 showed detectable H3K36me2 demethylase activity *in vitro* (Hsia *et al.*, 2010). In combination with our results, these findings suggest that the fragment containing amino-acid residues 101–140 is critical for the demethylation activity of JMJD5.

However, recent reports demonstrated that JMJD5 was unable to demethylate methylated histone peptides (Del Rizzo *et al.*, 2012) and that the overexpression of JMJD5 in A549 cells had no effect on the global levels of monomethylated, dimethylated and trimethylated histone H3K36, indicating that the function of JMJD5 was independent of the histone demethylase activity (Wang *et al.*, 2012). In addition, mouse JMJD5 (referred to as mJMJD5), which shares 78% amino-acid sequence identity with human JMJD5,

shows no demethylase activity either *in vitro* or *in vivo*. Furthermore, biochemical analysis revealed that mJMJD5 should be a protein hydroxylase (Youn *et al.*, 2012), implying that it is possible that human JMJD5 might function as a protein hydroxylase.

A search of the protein-structure database using the program *DALI* (Holm & Rosenström, 2010) revealed that the structure of JMJD5$^{176\text{-}C}$ is most similar to the structures of TYW5 (Z-score = 26.5; r.m.s.d. = 2.1 Å) and FIH (Z-score = 24.3; r.m.s.d. = 2.3 Å). In contrast to TYW5, which is an RNA hydroxylase, FIH is a well characterized JmjC-domain-containing protein hydroxylase that catalyses the hydroxylation of Asn803 of HIF-1α (Mahon *et al.*, 2001; Lando *et al.*, 2002). One significant difference between JMJD5 and FIH is that JMJD5 lacks the two C-terminal helices (αC1 and αC2) that mediate the dimerization of FIH (Figs. 5*a* and 5*c*). In addition, the conformations of several loops of JMJD5 differ from those in FIH (Fig. 5*a*). It has been shown that the Trp296 side chain of FIH blocks the binding of the methylated lysine residue and enables the binding pocket to accommodate an asparaginyl substrate (Mantri *et al.*, 2010; Elkins *et al.*, 2003). The corresponding residue in JMJD5 is Trp414, which might play the same role in blocking the binding of methylated lysines to the active site, together with Gln275 and Trp310, as described above (Figs. 5*b* and 5*c*). Moreover, in the structure of FIH in complex with the HIF-1α peptide, three residues, Tyr102, Arg238 and Gln239, are involved in directing Asn803 of HIF-1α to an accurate position in the active site (Elkins *et al.*, 2003). Among these, Tyr102 of FIH was shown to be critical for positioning the Asn803 side chain of HIF-1α in the

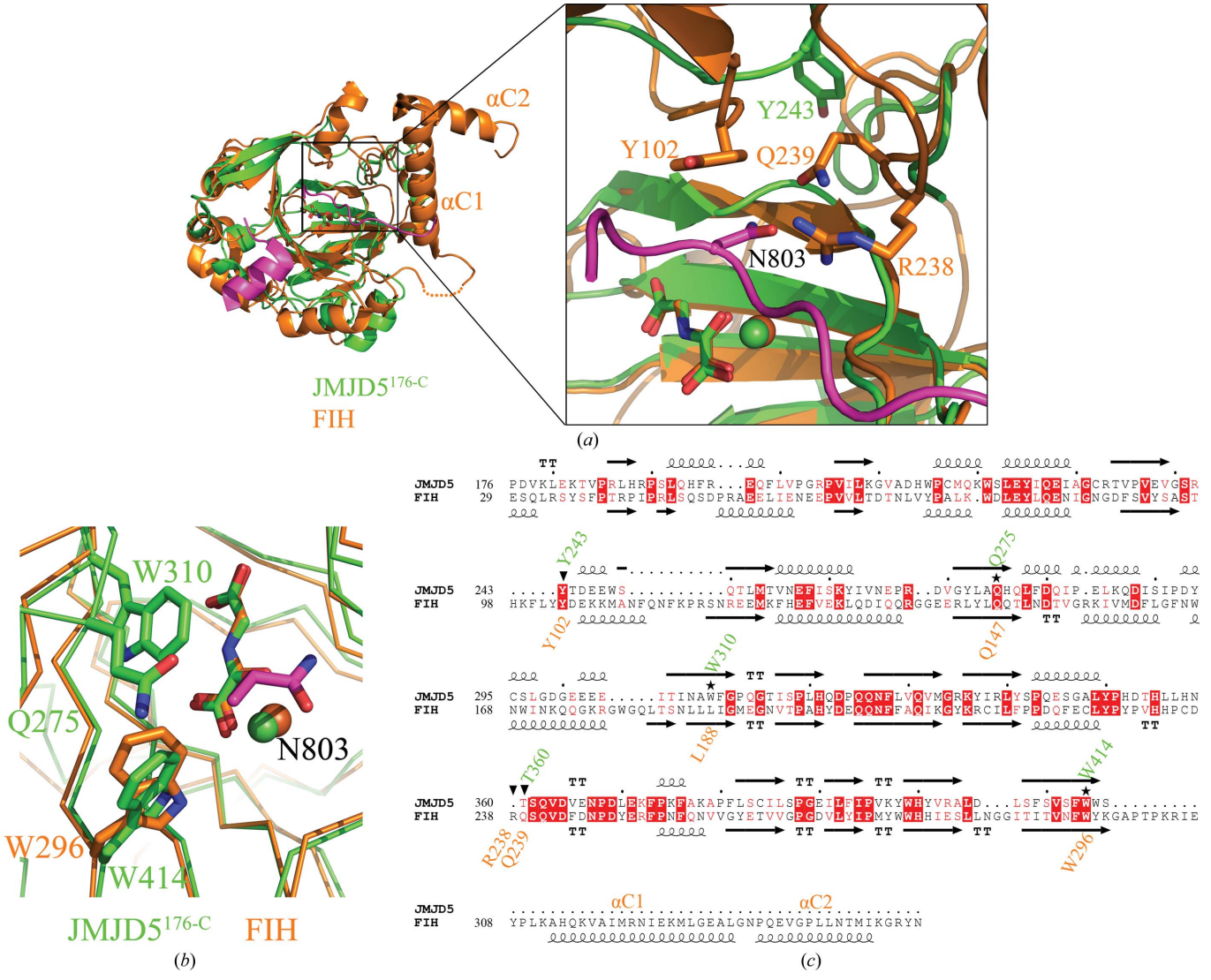

Figure 5
Structural comparison of JMJD5$^{176\text{-}C}$ with FIH. (*a*) Structural comparison of JMJD5$^{176\text{-}C}$ with FIH. An enlarged view of the substrate-binding site is shown on the right. (*b*) Detailed view of the active sites of JMJD5$^{176\text{-}C}$ and FIH. JMJD5$^{176\text{-}C}$ and FIH are shown as ribbon models. NOG and the residues are shown as stick models. Metal ions are shown as spheres. JMJD5$^{176\text{-}C}$, FIH and HIF-1α are coloured green, orange and magenta, respectively. (*c*) Structure-based sequence alignment of JMJD5$^{176\text{-}C}$ and FIH. The residues in JMJD5$^{176\text{-}C}$ blocking the insertion of the side chains of the methylated lysine residue and the residues in FIH involved in the interactions with Asn803 of the HIF peptide are numbered and marked by stars and triangles, respectively. The two C-terminal helices (αC1 and αC2) mediating the dimerization of FIH are labelled.

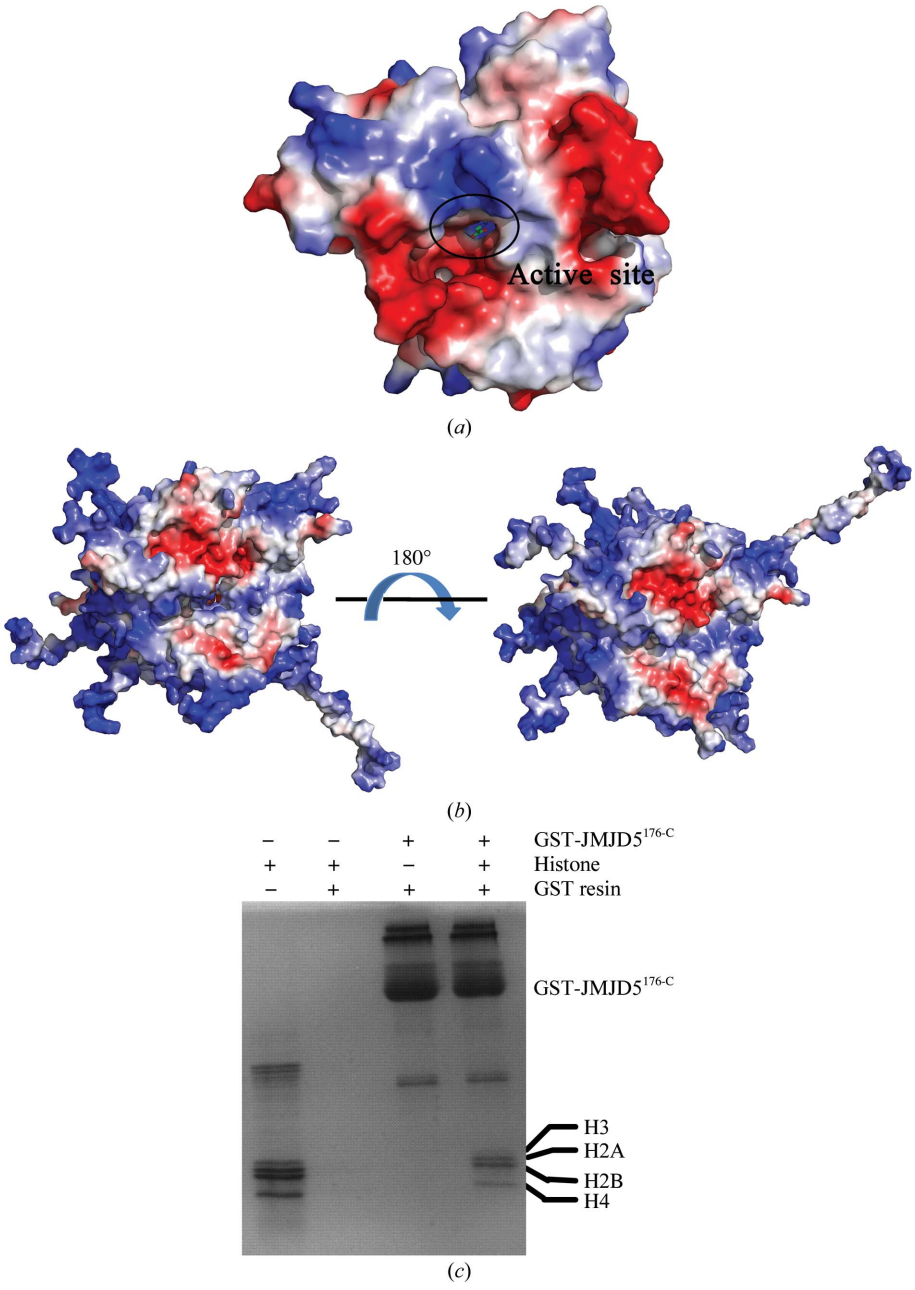

Figure 6
Interaction between JMJD5$^{176\text{-}C}$ and histone octamer proteins. Electrostatic surface representation of JMJD5$^{176\text{-}C}$ (*a*) and histone octamer proteins (*b*). Surfaces with a positive electrostatic potential are blue and those with a negative potential are red. NOG is shown as a stick model. (*c*) The interaction between JMJD5$^{176\text{-}C}$ and the histone octamer proteins was analysed using a GST pulldown assay.

3.4. Potential substrate for JMJD5

A large acidic surface area around the entrance of the active site of JMJD5$^{176\text{-}C}$ was identified *via* analysis of the electrostatic potential of the molecular surface (Fig. 6*a*). Because of the positively charged surface of histone proteins (Fig. 6*b*), we propose that JMJD5 might interact with core histone octamers. Consistent with our prediction based on structural analysis, it was shown that JMJD5$^{176\text{-}C}$ interacted with histone octamers using a GST pulldown assay (Fig. 6*c*). The binding of JMJD5$^{176\text{-}C}$ to the histone octamers indicated that the core histone octamers might be a potential substrate for JMJD5 to function as a protein hydroxylase.

Similar to JMJD5, JMJD6 is also a protein that contains only a JmjC domain. JMJD6 was first identified as a histone arginine demethylase for H3R2 and H4R3 (Chang *et al.*, 2007). However, in another report, JMJD6 was revealed to be a protein hydroxylase with U2AF65 (a protein associated with RNA splicing) as its substrate, instead of a histone demethylase (Webby *et al.*, 2009). In the work of Webby and coworkers, the hydroxylation of histone tails was detected *in vitro*. However, histones were not considered to be natural substrates of JMJD6. Recently, JMJD6 was characterized as a hydroxylase for histone tails using a new method: amino-acid composition analysis (Unoki *et al.*, 2013). The 5-hydroxylation of histone lysyl modified by JMJD6 inhibits the activity of the histone methyltransferase SMYD3 and the histone acetyltransferase P300, possibly by invading the active pockets of these enzymes and disturbing the formation of the active form of the substrate (Unoki *et al.*, 2013). In this study, we found that JMJD5 interacted with histone proteins and that JMJD5 might act as a protein hydroxylase. We propose that JMJD5 might hydroxylate the lysine residues of histone proteins and affect the function of other histone-modifying enzymes. Our work provides new clues to the study of the function of JMJD5.

binding pocket. In the structure of JMJD5, Tyr243 is located adjacent to the loop connecting $\beta3$ and $\beta4$. Although the position of Tyr243 of JMJD5 is opposite that of Tyr102 of FIH, it cannot be ruled out that the conformation of the loop connecting $\beta3$ and $\beta4$ might change upon substrate binding and thus direct Tyr243 to the correct position (Figs. 5*a* and 5*c*). In summary, the comparison of the structure of JMJD5 with that of FIH revealed that JMJD5 might function as a protein hydroxylase.

We thank the staff at beamline BL17U1 of the Shanghai Synchrotron Radiation Facility for assistance with data collection. We thank Professor Yunyu Shi for kindly providing

the calf thymus bulk histones. We also thank Dr Jianbin Ruan for critical reading and suggestions during the preparation of the manuscript. This work was supported by grants from the Chinese Ministry of Science and Technology (Nos. 2009CB825502 and 2012CB917202), the PhD Programs Foundation of the Ministry of Education of China (No. 20113402110033), the National Natural Science Foundation of China (Nos. 31171241 and 30970576) and the '100 Talents Program' of the Chinese Academy of Sciences to JZ.

References

Adams, P. D., Grosse-Kunstleve, R. W., Hung, L.-W., Ioerger, T. R., McCoy, A. J., Moriarty, N. W., Read, R. J., Sacchettini, J. C., Sauter, N. K. & Terwilliger, T. C. (2002). *Acta Cryst.* D**58**, 1948–1954.

Bannister, A. J., Schneider, R., Myers, F. A., Thorne, A. W., Crane-Robinson, C. & Kouzarides, T. (2005). *J. Biol. Chem.* **280**, 17732–17736.

Battye, T. G. G., Kontogiannis, L., Johnson, O., Powell, H. R. & Leslie, A. G. W. (2011). *Acta Cryst.* D**67**, 271–281.

Berdasco, M., Ropero, S., Setien, F., Fraga, M. F., Lapunzina, P., Losson, R., Alaminos, M., Cheung, N.-K., Rahman, N. & Esteller, M. (2009). *Proc. Natl Acad. Sci. USA*, **106**, 21830–21835.

Cao, R. & Zhang, Y. (2004). *Curr. Opin. Genet. Dev.* **14**, 155–164.

Carrozza, M. J., Li, B., Florens, L., Suganuma, T., Swanson, S. K., Lee, K. K., Shia, W.-J., Anderson, S., Yates, J., Washburn, M. P. & Workman, J. L. (2005). *Cell*, **123**, 581–592.

Chang, B., Chen, Y., Zhao, Y. & Bruick, R. K. (2007). *Science*, **318**, 444–447.

Del Rizzo, P. A., Krishnan, S. & Trievel, R. C. (2012). *Mol. Cell. Biol.* **32**, 4044–4052.

Elkins, J. M., Hewitson, K. S., McNeill, L. A., Seibel, J. F., Schlemminger, I., Pugh, C. W., Ratcliffe, P. J. & Schofield, C. J. (2003). *J. Biol. Chem.* **278**, 1802–1806.

Emsley, P. & Cowtan, K. (2004). *Acta Cryst.* D**60**, 2126–2132.

Evans, P. (2006). *Acta Cryst.* D**62**, 72–82.

Holm, L. & Rosenström, P. (2010). *Nucleic Acids Res.* **38**, W545–W549.

Horton, J. R., Upadhyay, A. K., Qi, H. H., Zhang, X., Shi, Y. & Cheng, X. (2010). *Nature Struct. Mol. Biol.* **17**, 38–43.

Hou, H. & Yu, H. (2010). *Curr. Opin. Struct. Biol.* **20**, 739–748.

Hsia, D. A., Tepper, C. G., Pochampalli, M. R., Hsia, E. Y.-C., Izumiya, C., Huerta, S. B., Wright, M. E., Chen, H.-W., Kung, H.-J. & Izumiya, Y. (2010). *Proc. Natl Acad. Sci. USA*, **107**, 9671–9676.

Huang, N., vom Baur, E., Garnier, J.-M., Lerouge, T., Vonesch, J.-L., Lutz, Y., Chambon, P. & Losson, R. (1998). *EMBO J.* **17**, 3398–3412.

Ishimura, A., Minehata, K., Terashima, M., Kondoh, G., Hara, T. & Suzuki, T. (2012). *Development*, **139**, 749–759.

Jones, M. A., Covington, M. F., DiTacchio, L., Vollmers, C., Panda, S. & Harmer, S. L. (2010). *Proc. Natl Acad. Sci. USA*, **107**, 21623–21628.

Jones, M. A. & Harmer, S. (2011). *Plant Signal. Behav.* **6**, 445–448.

Klose, R. J., Kallin, E. M. & Zhang, Y. (2006). *Nature Rev. Genet.* **7**, 715–727.

Lando, D., Peet, D. J., Gorman, J. J., Whelan, D. A., Whitelaw, M. L. & Bruick, R. K. (2002). *Genes Dev.* **16**, 1466–1471.

Laskowski, R. A., MacArthur, M. W., Moss, D. S. & Thornton, J. M. (1993). *J. Appl. Cryst.* **26**, 283–291.

Li, B., Howe, L., Anderson, S., Yates, J. R. III & Workman, J. L. (2003). *J. Biol. Chem.* **278**, 8897–8903.

Mahon, P. C., Hirota, K. & Semenza, G. L. (2001). *Genes Dev.* **15**, 2675–2686.

Mantri, M., Krojer, T., Bagg, E. A., Webby, C. J., Butler, D. S., Kochan, G., Kavanagh, K. L., Oppermann, U., McDonough, M. A. & Schofield, C. J. (2010). *J. Mol. Biol.* **401**, 211–222.

Martin, C. & Zhang, Y. (2005). *Nature Rev. Mol. Cell Biol.* **6**, 838–849.

McCoy, A. J., Grosse-Kunstleve, R. W., Adams, P. D., Winn, M. D., Storoni, L. C. & Read, R. J. (2007). *J. Appl. Cryst.* **40**, 658–674.

Murshudov, G. N., Skubák, P., Lebedev, A. A., Pannu, N. S., Steiner, R. A., Nicholls, R. A., Winn, M. D., Long, F. & Vagin, A. A. (2011). *Acta Cryst.* D**67**, 355–367.

Ng, H. H., Robert, F., Young, R. A. & Struhl, K. (2003). *Mol. Cell*, **11**, 709–719.

Otwinowski, Z. & Minor, W. (1997). *Methods Enzymol.* **276**, 307–326.

Ruan, J., Ouyang, H., Amaya, M. F., Ravichandran, M., Loppnau, P., Min, J. & Zang, J. (2012). *PLoS One*, **7**, e35376.

Sinha, K. M., Yasuda, H., Coombes, M. M., Dent, S. Y. & de Crombrugghe, B. (2010). *EMBO J.* **29**, 68–79.

Tachibana, M., Sugimoto, K., Nozaki, M., Ueda, J., Ohta, T., Ohki, M., Fukuda, M., Takeda, N., Niida, H., Kato, H. & Shinkai, Y. (2002). *Genes Dev.* **16**, 1779–1791.

Tsukada, Y., Fang, J., Erdjument-Bromage, H., Warren, M. E., Borchers, C. H., Tempst, P. & Zhang, Y. (2006). *Nature (London)*, **439**, 811–816.

Unoki, M., Masuda, A., Dohmae, N., Arita, K., Yoshimatsu, M., Iwai, Y., Fukui, Y., Ueda, K., Hamamoto, R., Shirakawa, M., Sasaki, H. & Nakamura, Y. (2013). *J. Biol. Chem.* **288**, 6053–6062.

Wagner, E. J. & Carpenter, P. B. (2012). *Nature Rev. Mol. Cell Biol.* **13**, 115–126.

Wang, Z., Wang, C., Huang, X., Shen, Y., Shen, J. & Ying, K. (2012). *Biochim. Biophys. Acta*, **1824**, 692–700.

Webby, C. J. *et al.* (2009). *Science*, **325**, 90–93.

Whetstine, J. R., Nottke, A., Lan, F., Huarte, M., Smolikov, S., Chen, Z., Spooner, E., Li, E., Zhang, G., Colaiacovo, M. & Shi, Y. (2006). *Cell*, **125**, 467–481.

Winn, M. D. *et al.* (2011). *Acta Cryst.* D**67**, 235–242.

Xiao, T., Hall, H., Kizer, K. O., Shibata, Y., Hall, M. C., Borchers, C. H. & Strahl, B. D. (2003). *Genes Dev.* **17**, 654–663.

Yang, Y. *et al.* (2010). *Cell Res.* **20**, 886–898.

Youn, M.-Y., Yokoyama, A., Fujiyama-Nakamura, S., Ohtake, F., Minehata, K., Yasuda, H., Suzuki, T., Kato, S. & Imai, Y. (2012). *J. Biol. Chem.* **287**, 12994–13004.